Circuit Model for Multiple Transverse Mode Vertical-Cavity Surface-Emitting Lasers

Tamás Marozsák, *Member, IEEE*

***Abstract*—The modeling of multimode operation in vertical-cavity surface-emitting laser diodes is difficult because spatial interaction between modes makes the problem very complex. In this paper, a novel circuit model is presented for such lasers, which is based on spatially dependent rate equations, and thus spatial hole burning and carrier diffusion are taken into account. These effects are studied in direct-modulated microwave vertical-cavity surface-emitting lasers by showing linear and nonlinear simulation examples in both time and frequency domains.**

***Index Terms*—Analog modulation, circuit model, diffusion, nonlinear, spatial hole burning, vertical-cavity surface-emitting lasers (VCSELs).**

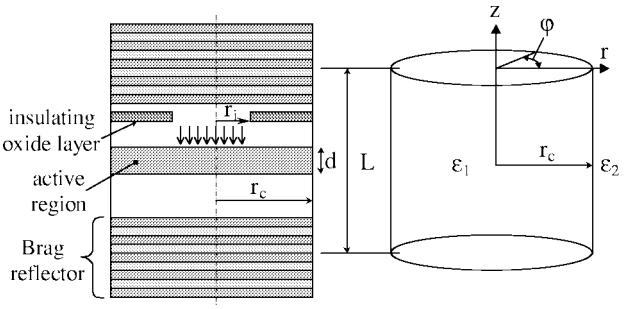

Fig. 1. VCSEL cavity.

I. Introduction

VERTICAL-CAVITY surface-emitting lasers (VCSELs) are very important light sources in optical communications. Their characteristics are very close to high-performance edge-emitting laser characteristics with low distortion, high modulation bandwidth, and high dynamic range [1], [2]. Their accurate modeling is important for both device engineers and circuit designers. The first one needs a model that simulates complex physical phenomena, resulting in long simulation time. The second one needs a much simpler, but relatively accurate model implemented in a circuit simulator with fast simulation time. The model presented here is in between: it can be used in conventional circuit simulators, and the simulation time is short, yet multiple lasing modes are simulated with interaction mechanisms between modes, such as spatial hole burning and carrier diffusion. Based on this model, fast modeling of multimode dynamics and nonlinear modulation characteristics are possible. This is important in direct-modulated microwave optical links where the laser characteristics determine intermodulation and dynamic range.

Simulating multimode operation in semiconductor lasers is usually done in two ways. In the first method, the rate equations are written in a spatially dependent form and are solved by a numerical method, such as in [3] and [4]. Because the rate equations must be solved in many spatial points, the problem becomes technically rather difficult, which means long calculation time. On the other hand, the results can provide deep information as well, such as accurate carrier and photon density distribution in the laser cavity [5]. The second method operates with phenomenological simplifications to avoid solving the rate equations in several spatial points. This was applied mainly to in plane multiple longitudinal mode (MLM) lasers. The simulation time is several orders less, and this way, even large signal dynamic operation can be simulated easily. These models are appropriate for mapping into circuit equivalents [6], [7] and for using in circuit simulator programs where static, small signal dynamic, and transient or large signal nonlinear behavior can be studied. In the following, a method is shown that is a mixture of these two: a circuit model is built for solving spatially dependent multimode rate equations.

The sections are organized as follows. In Section II, the mathematical model and the method of simplifying the spatial problem without heuristics is shown. In Section III, a novel equivalent circuit is shown which can model several numbers of modes. Section IV shows simulation results and explains the effect of diffusion and spatial hole burning. Section V concludes the paper.

II. Multimode VCSEL Model

A. Rate Equations

The mathematical model that will be used here for describing the dynamics of carriers and photons in the laser is based on the well-known rate equations. VCSELs are special lasers in two aspects: their cavity is cylindrical, and their longitudinal size is very small; therefore, they generally operate in only one longitudinal but several transversal modes. These modes share the same carrier population, having time-varying distribution. This results in time-varying coupling between them. Therefore, spatial dependence of the carrier density must be taken into account in the rate equations.

Fig. 1 shows a typical VCSEL structure where an oxide window is used to confine carriers in the active region. In the figure, L is effective cavity length, r_c is cavity radius, r_i is the

Manuscript received April 17, 2003; revised September 20, 2003. This work was supported in part by the European Union under COST 268 and 288 actions and by the Hungarian National Scientific Research Fund under "OTKA" T-030148 and T-042557.

The author is with the Department of Broadband Infcommunication Systems, Budapest University of Technology and Economics, Budapest H-1111, Hungary (e-mail: marozsak@mht.bme.hu).

Digital Object Identifier 10.1109/JLT.2003.819803

radius of current injection aperture, $\varepsilon 1$ and $\varepsilon 2$ are dielectric constants of the cavity and cladding, and d is the active region thickness.

Because of the cylindrical cavity, cylindrical coordinates are chosen. In the z direction, the active region is assumed to be uniform; therefore, there is no z dependence in the rate equations, as follows:

$$\frac{dn(t,r,\varphi)}{dt} = \frac{i(t,r,\varphi)}{q\cdot d} - \frac{n(t,r,\varphi)}{\tau_e} - v_g\cdot g(t,r,\varphi)\cdot p(t,r,\varphi) \quad (1)$$

$$\frac{dp(t,r,\varphi)}{dt} = v_g\cdot g(t,r,\varphi)\cdot p(t,r,\varphi) - \frac{p(t,r,\varphi)}{\tau_p} - \beta\cdot\frac{N}{\tau_e} \quad (2)$$

where t is time, r and φ are cylindrical coordinates, n and p are carrier and photon densities, i is current density, τ_e and τ_p are carrier and photon lifetimes, g is local optical gain, β is the spontaneous emission factor, N is the total carrier number in the cavity, q is the electron charge, and v_g is the group velocity. This system of equations contains several simplifications which are often used in the literature [4], [8]–[10]. Namely, the electron recombination processes are represented simply by electron lifetime, linear optical gain approximation will be used, and the spontaneous emission is uniformly distributed over the cavity independent of carrier distribution. Temperature effects will be also neglected. These simplifications are necessary to get linear interdependencies later in the final equations.

B. Spatial Dependence

Equations (1) and (2) must be solved so that they can be implemented in a circuit simulator. This means that only time (or frequency) can be an independent parameter, and space has to be eliminated. This can be done by separating time and space dependence in the equations. Two sets of orthogonal functions must be chosen for the photon and the carrier densities, and their weighted sum will give the total spatial distributions. The time variation of weights, or amplitudes, will give the time dependence.

For photons, the mode functions can be chosen, and using the modal gain formulation, one can write separate photon number rate equations for every lasing mode , as in [4], [8], and [10]. The electric-field-mode profile can be found by solving the wave equations in a cylindrical waveguide [11]. It is usually written in the form of (3), where J_m and K_m are Bessel functions of the first and second kind, and u and w are normalized lateral phase and attenuation constants, respectively. They can be calculated from the boundary conditions by solving the dispersion equation. If metal walls are used, u would equal the nth root of J_m, and u/r_c would be the cutoff wavenumber [12]

$$\Psi_{m,n}(r,\varphi) = \begin{cases} \frac{J_m\left(\frac{u\cdot r}{r_c}\right)\cdot\cos(m\cdot\varphi)}{J_m(u)}, & r\le r_c \\ \frac{K_m\left(\frac{w\cdot r}{r_c}\right)\cdot\cos(m\cdot\varphi)}{K_m(w)}, & r> r_c. \end{cases} \quad (3)$$

The indexes m and n denote the number of periods in φ and r directions, and the modes are labeled $\mathrm{LP}_{m,n}$. Fig. 2 shows some of the lowest order modes in a cylindrical cavity.

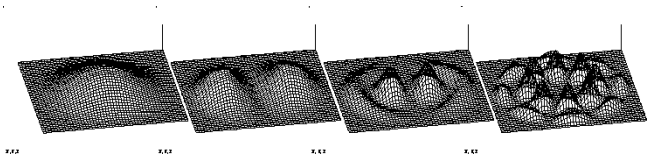

Fig. 2. Calculated intensity profile of VCSEL modes LP_{01}, LP_{11}, LP_{12}, and LP_{42}.

According to (3), the azimuthal dependence of the field functions is $\cos(m\varphi)$. This is separable when integrating over space and will become a multiplication by a constant. Therefore, eliminating the azimuthal dependence does not considerably affect the generality of the model. Using a one-dimensional electric-field-mode profile, the normalized intensity mode profile is defined as

$$\Theta_i(r) = \frac{\Psi_i^2(r)}{\int_0^\infty \Psi_i^2(r)\cdot r\, dr}. \quad (4)$$

Using this, the photon density in the active region can be expressed as

$$p_i(r) = \frac{P_i\Theta_i(r)}{\pi L} \quad (5)$$

where P_i is the total photon number in the ith mode. P_i will be the time-dependent amplitude of the spatial functions Θ_i, and the total intensity can be found from ΣP_i. In (5), it is taken into account that in the active region, the photon density is approximately two times higher than the average photon density due to the optical standing wave in the laser cavity.

In order to find an appropriate function set for the carrier density, the lasing process must be looked at more closely. The current injection is supposed to be uniform over a disk area so that initially the current density increases uniformly in that area. As the first mode starts to lase, it reduces the carrier density not uniformly but in accordance with its intensity mode profile. This process makes a hole in the carrier density where the mode has maximum intensity. This spatial-hole-burning effect (SHB) plays an important role in the VCSEL's operation. SHB influences the starting of other lasing modes, which will change the carrier profile in the same manner. This implies that the resulting carrier density will be correlated with the photon density functions; therefore, the function set should be able to write the photon intensity mode profiles efficiently. This can be achieved by defining the carrier density base functions as in [8], [13], and [14], as follows:

$$\Phi_j(r) = J_0\left(\frac{\gamma_j r}{R}\right) \quad (6)$$

where J_0 is the zero-order Bessel function, R is the radius normalizing parameter. It will equal the cavity radius as a first approximation. These functions are orthogonal if γ_j equals the jth root of J_1, the first-order Bessel function

$$\int_0^R J_0\left(\frac{\gamma_i r}{R}\right)\cdot J_0\left(\frac{\gamma_j r}{R}\right)\cdot r\cdot dr = \begin{cases} 0, & i\ne j \\ \frac{R^2}{2}J_0^2(\gamma_i), & i=j\,. \end{cases} \quad (7)$$

Defining n_j as the time-dependent amplitude of the jth carrier density function $\Phi_j(r)$, the total carrier density can be expressed as

$$n(r) = \sum n_j \Phi_j(r). \tag{8}$$

Substituting (5) and (8) into the rate equations (1) and (2), assuming uniformity in the φ direction, multiplying one by one with each of the base functions, and integrating over the cavity volume, the spatially dependent equations can be expressed as two sets of spatially independent equations

$$\begin{aligned}\frac{dn_J}{dt} &= \frac{I \cdot c_J}{q\,d\,B_J} - \frac{v_g a}{\pi L B_J} \cdot \sum_i \sum_j n_J P_i g_{i,j,J} \\ &\quad + \frac{v_g a \cdot n_t}{\pi L B_J} \sum_i P_i g_{i,J} - \frac{n_J}{\tau_e} \qquad (9)\\ \frac{dP_i}{dt} &= v_g \Gamma_z a P_i \left(\sum_j n_j g_{i,j} - n_t \right) \\ &\quad + \beta \cdot \frac{N_e}{\tau_e} - \frac{P_i}{\tau_{p,i}} \qquad (10)\end{aligned}$$

where I is current density, a is differential gain, Γ_z is longitudinal confinement factor, $\tau_{p,i}$ is the photon lifetime in the ith mode. With the exception of B_J, the remaining constants represent overlap integrals and can be calculated according to (11). Equations (9) and (10) model the spatial processes by varying the spatial function amplitudes P_i and n_J in time; therefore, they have to be solved for time variation of P_i and n_J only.

$$\begin{aligned} g_{i,J} &= \int_0^R \Theta_i(r)\Phi_J(r) \cdot r\, dr \\ g_{i,j,J} &= \int_0^R \Phi_j(r)\Theta_i(r)\Phi_J(r) \cdot r\, dr \\ c_J &= \int_0^R i(r)\Phi_J(r) \cdot r\, dr \\ B_J &= \frac{R^2}{2} J_0^2(\gamma_J). \end{aligned} \tag{11}$$

The index J is used to differ from the index j used in the double sum in (9). Both can run from 0 to $(j_{\max} - 1)$, which depends on our decision as to how many base functions we use to describe the carrier distribution. The index i runs from 1 to $i_{\max}$, the number of possible lasing modes.

The necessity of $g_{i,j,J}$ is sometimes overlooked in the literature, or some kind of heuristic is used to avoid it [8]. In these cases, the total carrier distribution, given by (8), will not be correct, and in most cases, the result will have negative carrier-density regions.

As a result, we have $j_{\max}$ equations for carriers and $i_{\max}$ for photons. There are $j_{\max}B_J$ constants, $j_{\max}C_J$ constants, $j_{\max} \cdot i_{\max}g_{i,J}$ constants and $j_{\max}^2 \cdot i_{\max}g_{i,j,J}$ constants. The large number of constants is the price we have to pay for eliminating the spatial dependence from the original problem. However, if the constants are once determined, their usage speeds up the solution of the rate equations and makes their implementation in a circuit simulator possible.

C. Diffusion

Carrier diffusion is very important in VCSELs; therefore, it has to be taken into account in the model. The electron rate equation (1) must be extended by $+D\nabla^2 n(t,r,\varphi)$, where D is the diffusion constant, and ∇ is the Laplace operator. In cylindrical coordinates, the Laplace operator takes the form

$$\nabla^2 n(r,\varphi) = \frac{1}{r}\frac{\partial}{\partial r}\left(r \frac{\partial n(r,\varphi)}{\partial r} \right) \frac{1}{r^2} + \frac{\partial^2 n(r,\varphi)}{\partial \varphi^2}. \tag{12}$$

Applying the Laplace operator on the carrier distribution base functions (6) gives

$$\frac{1}{r}\frac{\partial}{\partial r}\left(r \frac{\partial}{\partial r} J_0\left(\frac{\gamma_j r}{R}\right)\right) = -\left(\frac{\gamma_j}{R}\right)^2 J_0\left(\frac{\gamma_j r}{R}\right). \tag{13}$$

Using this result in the carrier rate equation (9), we get

$$\begin{aligned}\frac{dn_J}{dt} &= \frac{Ic_J}{qdB_J} - \frac{n_J}{\tau_e} - \frac{v_g a}{\pi L B_J} \sum_i \sum_j n_J P_i g_{i,j,J} \\ &\quad + \frac{v_g a n_t}{\pi L B_J} \sum_i P_i g_{i,J} - D d_J n_J \end{aligned} \tag{14}$$

where $d_J = (\gamma_J/R)^2$. This implies that there are $j_{\max}$ new constants to determine before simulation.

III. Circuit Equivalent

Equations (10) and (14) define a system of first-order differential equations which can be solved by a circuit simulator. The equations have the form similar to $C(dV/dt) = I_1 + I_2 + \cdots$ (assuming $C = 1$), which is the Kirchoff equation for a circuit consisting of one capacitor and several current sources connected parallel. The photon number and the carrier density (P_i and n_J in the equations) can be represented by the voltage on the capacitor, and the rates can be represented by the currents. Using this idea, (10) and (14) can be modeled by the equivalent circuit network shown in Fig. 3. This electrical network consists of several subcircuits described previously. There are $i_{\max}$ subcircuits for representing the $i_{\max}$ number of photon equations and $j_{\max}$ subcircuits representing the $j_{\max}$ number of electron equations. Each circuit contains one capacitor and a number of voltage-controlled current sources equal to the number of terms on the right side of the equations. These terms are indicated in Fig. 3 below the generators. In these definitions, the names of currents refer to the physical process that they represent. $I_{\rm stim}$, $I_{\rm st}$, and $I_{\rm stx}$ mean different stimulated emission-rate terms; the other names are obvious. In each subcircuit, these currents are different as they are defined by constants having different i or J indexes. In the expressions, P_i and n_J become control voltages measured on the capacitors of the appropriate subcircuits (Vp_i and Vn_J). The input signal of the electrical network is given by I, which is common for the current sources defined by Ic_j/qdB_j in each electron subcircuit. In the simulation, the network is solved for voltages Vp_i and Vn_J, which represent the number of photons P_i in the given mode and the electron density function amplitudes n_J, respectively.

Altogether the network consists of $j_{\max}+i_{\max}$ capacitors and $j_{\max} \cdot (2 + i_{\max} + i_{\max} \cdot j_{\max}) + i_{\max} \cdot (2 + j_{\max})$ voltage-controlled current sources. This can be a large number if many optical modes are allowed and many electron density functions have to be used. Fortunately, the carrier density base functions

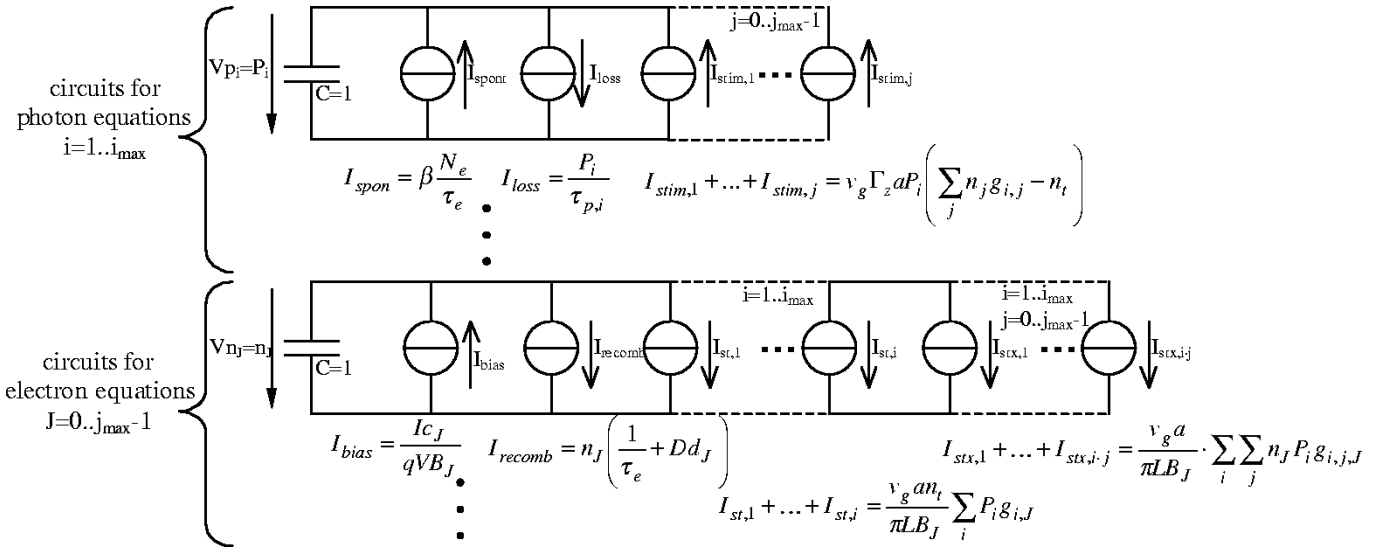

$$I_{spon} = \beta \frac{N_e}{\tau_e} \quad I_{loss} = \frac{P_i}{\tau_{p,i}} \quad I_{stim,1} + \ldots + I_{stim,j} = v_g \Gamma_z a P_i \left(\sum_j n_j g_{i,j} - n_t \right)$$

$$I_{bias} = \frac{Ic_J}{qVB_J} \quad I_{recomb} = n_J \left(\frac{1}{\tau_e} + Dd_J \right)$$

$$I_{stx,1} + \ldots + I_{stx,i\cdot j} = \frac{v_g a}{\pi L B_J} \cdot \sum_i \sum_j n_J P_i g_{i,j,J}$$

$$I_{st,1} + \ldots + I_{st,j} = \frac{v_g a n_t}{\pi L B_J} \sum_i P_i g_{i,J}$$

Fig. 3. Equivalent circuit for solving the multimode VCSEL rate equations.

defined in (6) work very well in practice. As a result, a few carrier density functions are usually sufficient to get satisfying results. This means that a low value for $j_{\max}$ is usually appropriate.

In sophisticated simulator languages, such as APLAC, it is possible to use FOR-NEXT loops in the circuit definition and define the ladder structures in Fig. 3 automatically. The overlap constants of (11) are calculated once before the simulation and stored in a separate file. The simulation file reads these constants and uses them in the circuit definition.

Circuit simulators converge best if the currents and voltages are in the usual range, which is from 10^{-12} to 10^{3}. Therefore, the voltages and currents in the equivalent network have to be scaled to fall into that range. This was done by multiplying the current of the generators and node voltages by an appropriate value.

The electric network of Fig. 3 solves (10) and (14), which represents the intrinsic part of a laser diode. It does not include real diode parasitics such as leakage currents and diode behavior. However, it could be included easily by controlling the bias-current generators with a current measured on a diode connected to all of the parasitic circuit elements. The extrinsic laser model can be very simple above threshold [15]; only some capacitors and resistors are needed to add to the intrinsic laser.

IV. Simulation Results

The validity of the model and the circuit equivalent were checked by comparison to other models. The COST 268 action of the European Union had an open forum for comparing simulation results obtained from the same input parameters. The physical parameters of the laser for the following simulations were chosen from the modeling exercise of the action. The parameters are listed in Table I.

In the laser structure, two optical modes were possible which set $i_{\max}$ to 2. The mode profiles were *a priori* known from optical field simulations and are shown in Fig. 4. The carriers were allowed outside the r_c cavity radius; therefore, $R = 2r_c$ was chosen in (6) for proper simulation of diffusion. In most cases,

TABLE I
Laser Parameters for Simulations

Name	Symbol	Value
cavity radius	r_c	3.4 μm
oxide window radius	r_i	3 μm
active region thickness	d	5 nm
longitudinal confinement factor	Γ_z	$7.922 \cdot 10^{-3}$
electron charge	q	$1.6 \cdot 10^{-19}$ C
electron lifetime	τ_e	0.9794 ns
group velocity	vg	$0.07138 \cdot 10^{9}$ m/s
gain const. (=diff. gain)	a	$6.456 \cdot 10^{-20}$ m^2
mirror refl. for mode 1	$\alpha_{m,1}$	$9.0886 \cdot 10^{2}$ 1/m
mirror refl. for mode 2	$\alpha_{m,2}$	$10.1672 \cdot 10^{2}$ 1/m
photon lifetime in mode 1	$\tau_{p,1}$	15.414 ps
photon lifetime in mode 2	$\tau_{p,2}$	13.779 ps
carrier density at transp.	n_t	$1.267 \cdot 10^{24}$ 1/m^3
spont. em. factor	β	$1 \cdot 10^{-5}$
diffusion constant	D	$1 \cdot 10^{-3}$m^2/s

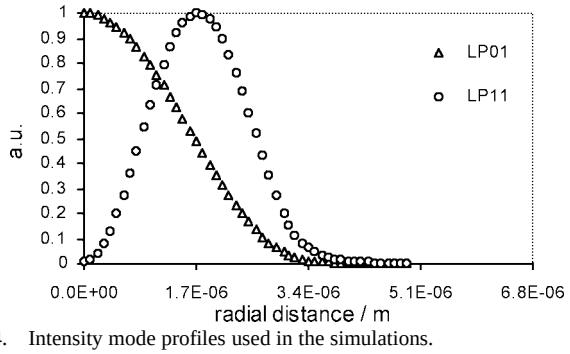

Fig. 4. Intensity mode profiles used in the simulations.

using five base functions for the carrier density gives good results, but here, $j_{\max} = 11$ was chosen for getting very accurate carrier distribution.

Fig. 5(a) shows the result of dc simulations in several bias points, sweeping from 0–400 μA. It can be seen that lasing starts at $I_{\rm th} = 93$ μA with the $\rm LP_{01}$ mode. As the optical intensity increases in this mode, a hole is created in the carrier distribution at $r = 0$, as shown in Fig. 5(b). This affects the start of $\rm LP_{11}$ mode at $I = 256$ μA. Fig. 5(b) also shows that diffusion causes

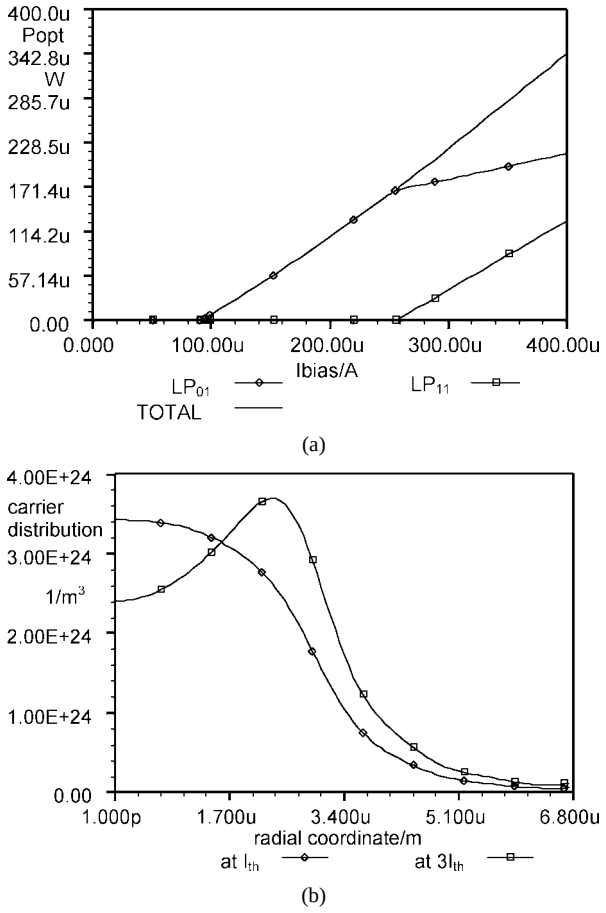

Fig. 5. (a) Result of dc simulation: bias current versus optical power. (b) Result of dc simulation: carrier distribution at $I_{\rm th}$ and $3I_{\rm th}$.

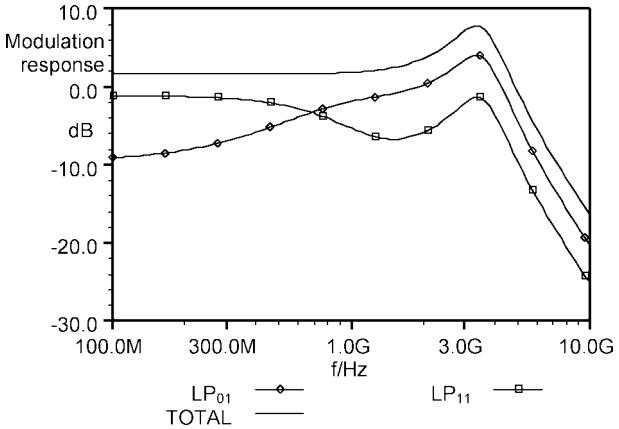

Fig. 6. Result of ac simulation; modulation response of modes at $3I_{\rm th}$.

high electron density outside of the $r_i = 3$ μm current aperture, which is also important in starting the $\rm LP_{11}$ mode.

Fig. 6 shows the small signal modulation response for each mode and for total intensity as result of ac simulation. In [10], it is emphasized that the total modulation response is not a simple sum of modulation responses of separate modes, since their responses are not necessarily in phase. In this model, the ac node voltages, representing photon number dynamics, are easy to sum as complex values. Optical power is calculated afterwards, which always gives the correct value. Strong antiphase

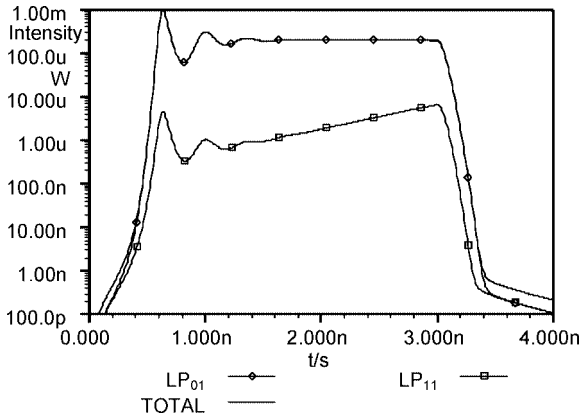

Fig. 7. Result of transient simulation, response to a $3I_{\rm th}$ current pulse with 0 s–3 ns duration.

behavior of modes, such as in [10], could not be observed here; the maximum phase difference was about 50°. Similar results were achieved when the simulation was repeated with an annular current distribution resulting in $\rm LP_{11}$ and $\rm LP_{21}$ operating modes, which overlap more than $\rm LP_{01}$ and $\rm LP_{11}$.

In Fig. 6, the $\rm LP_{11}$ mode has a stronger modulation response than the $\rm LP_{01}$ mode up to 700 MHz; then, the opposite becomes true. This frequency depends on the diffusion constant D, which determines how fast the diffusion can follow the modulation. At higher modulation frequencies, the $\rm LP_{11}$ mode cannot gain from the diffusion effect, and its response to modulation decreases.

The diffusion effect can be seen in Fig. 7 as well, where the transient behavior is simulated. As the current pulse starts, the current distribution prefers the $\rm LP_{01}$ mode. Then the spatial hole in the carrier distribution shown in Fig. 5(b) develops and together with diffusion it causes high carrier density where $\rm LP_{11}$ has maximum intensity; so it starts to lase. Its intensity increases slowly as diffusion provides a slow increase in carrier density. Fig. 5(a) showed that at $3I_{\rm th}$ ($\sim$280 μA), the optical power is approximately 20 μW in the $\rm LP_{11}$ mode in steady state. This power could not be reached in 3 ns in Fig. 7 due to the high diffusion constant. The relaxation oscillation of the curves does not show antiphase properties of the two modes. This is in agreement with the ac simulation.

The last and most important result of the paper is shown in Fig. 8, the results of a single-tone harmonic balance simulation. Up to the fifth harmonic of the modulating tone, at frequency f_m, was taken into account, but only the second and third harmonic are presented as most important in applications of direct-modulated lasers. The amplitude of the modulating signal was $I_{\rm bias}/10$, and the bias point was $3I_{\rm th}$. In directly modulated transmission systems, the nonlinear behavior causes distortion and intermodulation. The generated second and third harmonic levels simulated here are in quantitative connection with the coefficients of the laser nonlinear characteristic and, hence, have special importance.

The curves show that the laser nonlinearity is increasing toward the relaxation oscillation frequency in agreement with theory. It also can be seen that diffusion affects the higher order harmonics similar to the way it affects the fundamental one. The modulation response for f_m agrees with the result of the small

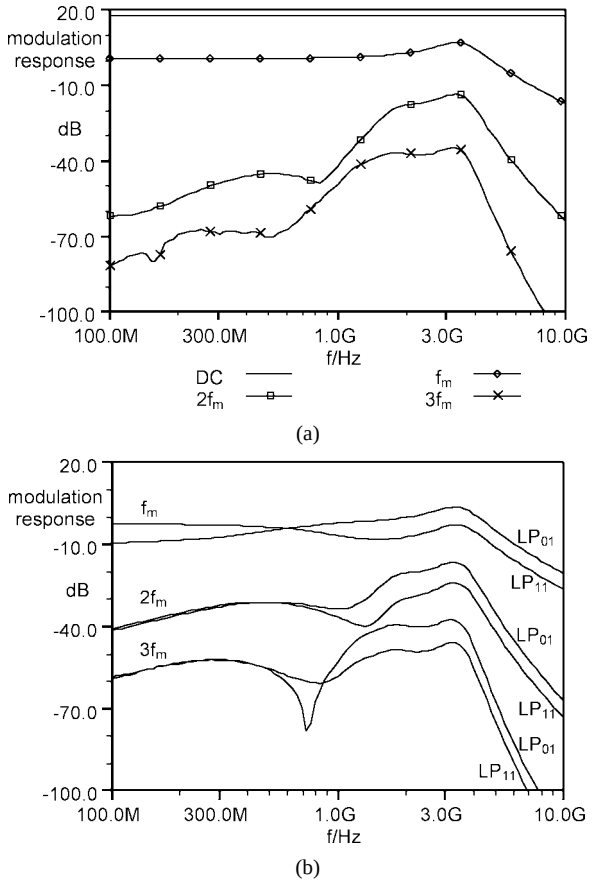

Fig. 8. (a) Result of one tone harmonic balance simulation, with modulation responses of harmonics. (b) Result of one tone harmonic balance simulation, with intensity versus frequency in each mode separately.

signal (ac) analyzes in Fig. 6. As the modulating frequency becomes higher than approximately 700 MHz, the LP_{11} response decreases in all higher order harmonics as well. This can be important in analog application of VCSELs because external reflectivity, such as a coupling fiber or a photodetector surface, can enhance one mode, causing the modulation proprieties to change severely. These diffusion-induced modes should be avoided in properly designed VCSELs. A low optical reflection environment is needed, even when these modes exist with low optical power.

V. Conclusion

A novel equivalent circuit for modeling multiple transversal mode behavior in VCSELs was presented. Elimination of spatial dependence from the rate equations by calculating overlap integrals and the definition of an equivalent circuit using these constants were shown. This method made it possible to simulate the multimode operation of VCSELs in circuit simulators. The main advantage of the model is that the wide variety of analyses methods implemented in circuit simulators can be applied to the system. In this way, the study of linear and nonlinear dynamic behavior of such lasers is possible. This is important in microwave optical links. Simulations have shown that the model was in agreement with other mathematical models. The results of dc, ac, transient, and single-tone harmonic balance simulations were presented, and the effect of diffusion was studied on the results in the linear and nonlinear regime. It was shown that the diffusion-induced modes have slow dynamics in both regimes. This needs attention in the design and application of these lasers in directly modulated optical links.

Acknowledgment

The author would like to thank T. Berceli and R. Satz for the valuable discussions.

References

[1] T. Marozsák *et al.*, "Direct modulated lasers in radio over fiber applications," in *Tech. Dig. Int. Topical Meeting Microwave Photonics*, 2002, pp. 129–132.

[2] C. Carlsson *et al.*, "Analog modulation properties of oxide confined VCSEL's at microwave frequencies," *J. Lightwave Technol.*, vol. 20, pp. 1740—1749, Sept. 2002.

[3] J. W. Scott *et al.*, "Modeling temperature effects and spatial hole burning to optimize vertical-cavity," *IEEE J. Quantum Electron.*, vol. 29, pp. 1295–1308, May 1993.

[4] A. Valle *et al.*, "Spatial hole burning effects on the dynamics of vertical cavity surface-emitting laser diodes," *IEEE J. Quantum Electron.*, vol. 31, pp. 1423–1431, Aug. 1995.

[5] C. H. Chong and J. Sarma, "Lasing mode selection in vertical-cavity surface-emitting laser diodes," *IEEE Photon. Technol. Lett.*, vol. 5, pp. 761–764, July 1993.

[6] I. Habermayer, "Nonlinear circuit model for semiconductor lasers," *Opt. Quantum Electron.*, vol. 13, 1981.

[7] W. Chen and S. Liu, "Circuit model for multilongitudinal-mode semiconductor lasers," *IEEE J. Quantum Electron.*, vol. 32, pp. 2128–2132, Dec. 1996.

[8] J. Dellunde *et al.*, "Statistics of transverse mode turn-on dynamics in VCSELs," *IEEE J. Quantum Electron.*, vol. 33, pp. 1197–1204, July 1997.

[9] L. A. Coldren and S. W. Corzine, *Diode Lasers and Photonic Integrated Circuits*. New York: Wiley, 1995.

[10] M. S. Torre and H. F. Ranea-Sandoval, "Modulation response of multiple transverse modes in vertical-cavity surface-emitting lasers," *IEEE J. Quantum Electron.*, vol. 36, pp. 112–117, Jan. 2000.

[11] M. Koshiba, *Optical Waveguide Analysis*. New York: McGraw-Hill, 1992.

[12] D. M. Pozar, *Microwave Engineering*. Reading, MA: Addison-Wesley, 1990.

[13] J. J. Morikuni *et al.*, "Spatially independent VCSEL models for the simulation of diffusive turn-off transients," *J. Lightwave Technol.*, vol. 17, Jan. 1999.

[14] S. F. Yu *et al.*, "Theoretical analysis of modulation response and second-order harmonic distortion in vertical-cavity surface-emitting lasers," *IEEE J. Quantum Electron.*, vol. 32, Dec. 1996.

[15] D. Wiedenmann *et al.*, "Design and analyzis of single-mode oxidized VCSELs for high-speed optical interconnects," *IEEE J. Select. Topics Quantum Electron.*, vol. 5, May/June 1999.

Tamás Marozsák (M'97) was born in Hungary in 1971. He received the M.Sc. degree in electrical engineering from the Technical University of Budapest, Budapest, Hungary, in 1995.

Since 1998, he has been an Assistant Professor with the Department of Broadband Infocommunication Systems, Budapest University of Technology and Economics, Budapest, Hungary. He is author or coauthor of more than 50 technical papers in the field of optical communications and microwave photonics.